

Disentangling orbital and spin exchange interactions for Co^{2+} on a rocksalt lattice

P. M. Sarte,^{1,2} R. A. Cowley,^{3,†} E. E. Rodriguez,⁴ E. Pachoud,^{1,2} D. Le,⁵ V. García-Sakai,⁵
 J. W. Taylor,⁵ C. D. Frost,⁵ D. Prabhakaran,³ C. MacEwen,⁶ A. Kitada,⁷ A. J. Browne,^{1,2}
 M. Songvilay,^{2,6} Z. Yamani,⁸ W. J. L. Buyers,^{8,9} J. P. Attfield,^{1,2} and C. Stock^{2,6}

¹*School of Chemistry, University of Edinburgh, Edinburgh EH9 3FJ, United Kingdom*

²*Centre for Science at Extreme Conditions, University of Edinburgh, Edinburgh EH9 3FD, United Kingdom*

³*Department of Physics, Clarendon Laboratory, University of Oxford,
 Park Road, Oxford, OX1 3PU, United Kingdom*

⁴*Department of Chemistry and Biochemistry, University of Maryland, College Park, Maryland 20742, USA*

⁵*ISIS Facility, Rutherford Appleton Laboratory, Chilton, Didcot OX11 0QX, United Kingdom*

⁶*School of Physics and Astronomy, University of Edinburgh, Edinburgh EH9 3FD, United Kingdom*

⁷*Department of Materials Science and Engineering,
 Kyoto University, Yoshida-honmachi, Sakyo, Kyoto 606-8501, Japan*

⁸*National Research Council, Chalk River, Ontario K0J 1J0, Canada*

⁹*Canadian Institute of Advanced Research, Toronto, Ontario M5G 1Z8, Canada*

(Dated: August 24, 2018)

Neutron spectroscopy was applied to study the magnetic interactions of orbitally degenerate Co^{2+} on a host MgO rocksalt lattice where no long range spin or orbital order exists. The paramagnetic nature of the substituted monoxide $\text{Co}_{0.03}\text{Mg}_{0.97}\text{O}$ allows for the disentanglement of spin-exchange and spin-orbit interactions. By considering the prevalent excitations from Co^{2+} spin pairs, we extract 7 exchange constants out to the fourth coordination shell. An antiferromagnetic next nearest neighbor 180° exchange interaction is dominant, however dual ferromagnetic and antiferromagnetic interactions are observed for pairings with other pathways. These interactions can be understood in terms of a combination of orbital degeneracy in the t_{2g} channel and the Goodenough-Kanamori-Anderson (GKA) rules. Our work suggests that such a hierarchy of exchange interactions exists in transition metal-based oxides with a t_{2g} orbital degeneracy.

I. INTRODUCTION:

The combination of magnetic exchange and orbital degeneracy has provided the basis for a number of topics in condensed matter physics including metal-insulator transitions, high temperature superconductors, colossal magnetoresistance,¹⁻³ and more recently Kitaev interactions⁴⁻⁶. Rocksalt CoO was the first orbitally degenerate compound to have its magnetic structure investigated using neutron diffraction,⁷⁻¹⁰ but the underlying exchange interactions are still not known. Indeed, calculations and experiment have been hindered by the complex electronic and orbital ground state of Co^{2+} . While e_g mediated magnetic exchange has been well understood (for example in KCuF_3 ¹¹), the case of exchange involving degenerate t_{2g} orbitals has proven more difficult.¹² We investigate the magnetic exchange interactions in the case of a t_{2g} orbital degeneracy by performing neutron spectroscopy on MgO substituted with Co^{2+} . We extract 7 exchange interactions and observe dual ferro and antiferromagnetic exchange interactions with comparable magnitudes. The dual exchange interactions is a direct result of the underlying t_{2g} orbital degeneracy of Co^{2+} .

The starting point for understanding the spin-orbital Hamiltonian for paramagnetic Co^{2+} ions is crystal field theory based on octahedral coordination^{13,14} (Fig. 1(a) for rocksalt CoO)¹⁵⁻¹⁷. As schematically shown in Fig. 1(b), the octahedral crystal field ($\hat{\mathcal{H}}_{CF}$) splits the 5 degenerate d -orbitals (4F) such that the d^7 electronic structure consists of 5 electrons occupying the lower energy t_{2g} states and 2 electrons in the higher energy e_g orbitals. This constitutes two orbital triplets ($^4T_{1,2}$) levels separated by $10Dq \sim 900$ meV¹⁷. The triplet degenerate 4T_1 ground state can be approximated to have an effective orbital angular momentum of $\tilde{l} = 1$.¹⁶⁻²⁴

Applying spin-orbit coupling (defined by $\hat{\mathcal{H}}_{S.O.} = \tilde{\lambda} \vec{l} \cdot \vec{S}$, with $S = \frac{3}{2}$) to this orbital ground state results in 3 effective spin-orbit manifolds classified by an effective angular momentum of $j_{\text{eff}} = \frac{1}{2}, \frac{3}{2}$ and $\frac{5}{2}$ (with $\vec{j}_{\text{eff}} = \vec{l} + \vec{S}$). The $j_{\text{eff}} = \frac{1}{2}$ ground state is separated from the higher energy $j_{\text{eff}} = \frac{3}{2}$ states by $\frac{3}{2} \tilde{\lambda} \sim 36$ meV¹⁷.

In the presence of long range magnetic order (as exists in CoO at low temperatures), the total single-ion Hamiltonian for Co^{2+} can then be summarized by

$$\hat{\mathcal{H}}_{SI} = \hat{\mathcal{H}}_{CF} + \hat{\mathcal{H}}_{S.O.} + \hat{\mathcal{H}}_{MF} \quad (1)$$

where $\hat{\mathcal{H}}_{CF}$, $\hat{\mathcal{H}}_{S.O.}$ and $\hat{\mathcal{H}}_{MF}$ are the octahedral crystal field, spin-orbit, and magnetic order induced molecular field. The effect of magnetic ordering on the three spin-orbit manifolds discussed above can be illustrated by considering a single dominant next nearest neighbor 180° Co^{2+} - O^{2-} - Co^{2+} superexchange J_2 with

$$\hat{\mathcal{H}}_{MF} = 2J_2 z_2 (\hat{\mathbf{S}})_{av} \hat{S}^z, \quad (2)$$

where z_2 and \hat{S}^z denote the number of Co^{2+} neighbors and the z -axis of the spin operator¹⁵. As illustrated in Fig. 1(c), by considering only the predicted value of J_2 by Kanamori¹⁶ in the mean field expression for $\hat{\mathcal{H}}_{MF}$, a complex admixture of different molecular field split Co^{2+} spin-orbit manifolds occurs in the presence of magnetic order¹⁵⁻¹⁷.

The strong magnetic ordered induced mixing of multiple j_{eff} manifolds in CoO is in contrast to many other Co^{2+} based magnets that have both weak exchange and molecular fields and thus exhibit weak mixing^{18,26-28}. CoO is further complicated by the possibility of multiple long-range spin-spin interactions²⁹⁻³². The extraction of

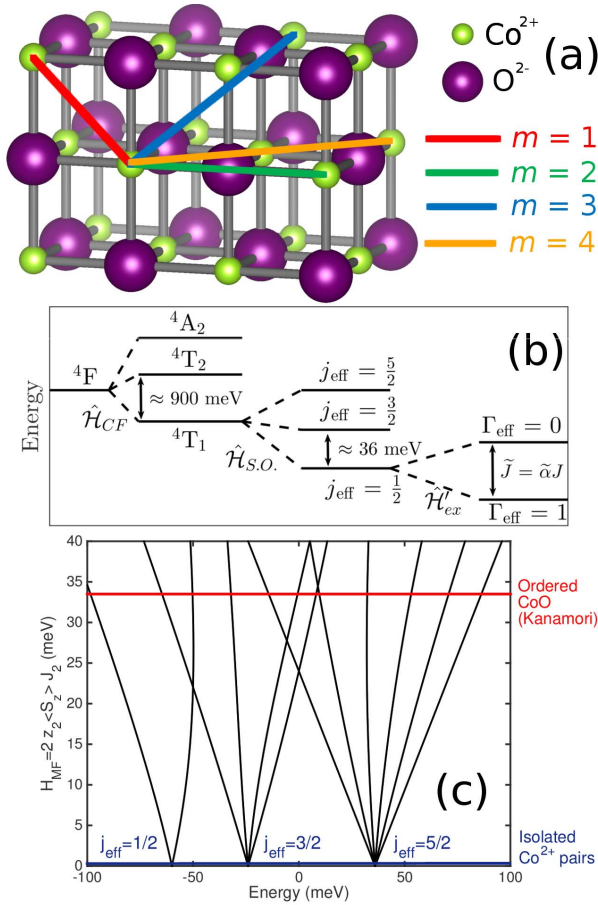


FIG. 1. (a) Cubic (room temperature) rock salt $Fm\bar{3}m$ crystal structure of CoO ²⁵. The pair distances between first shell (nearest) neighbors, second shell (next nearest) neighbors, *etc.* are denoted by $m = 1, 2, \text{etc.}$, respectively. (b) The effective pair Hamiltonian $\hat{\mathcal{H}}_{pair}$ for $\text{Co}_{0.03}\text{Mg}_{0.97}\text{O}$. (c) The energy eigenvalues of the single ion Hamiltonian including a molecular field from magnetic order with Kanamori's estimate¹⁶ of J_2 shown by the solid red line.

the multiple spin exchanges in CoO is thus experimentally very difficult despite the simplicity of its crystal structure^{15,17,22,23,30,31,33-35}.

We have extracted the magnetic exchange interactions on a rocksalt lattice by investigating weakly substituted $\text{Co}_{0.03}\text{Mg}_{0.97}\text{O}$ using neutron scattering and through considering excitations from the dominant Co^{2+} pair response. This paper is divided into four sections including this introduction. We first describe the experimental methods including materials preparation and characterization techniques where we conclude that our dilute sample can be described by a Co^{2+} pair response. An expanded description of the characterization is given in the Supplementary Information illustrating the x-ray, susceptibility, and EDX data.³⁶ In section three, the theory required to extract both the exchange constant and also the distance associated with the interaction is outlined. We then show the experimental data used to derive the exchange interactions. We finally conclude with a discussion of the results including a comparison with thermodynamic data from pure CoO and also how we can understand the results in terms of the GKA rules.

II. EXPERIMENTAL DETAILS AND MATERIALS CHARACTERIZATION:

To extract individual J constants for Co^{2+} , we have followed the pioneering work on dilute Mn^{2+} ^{37,38} and Co^{2+} ²² compounds and measured the dilute monoxide $\text{Co}_{0.03}\text{Mg}_{0.97}\text{O}$ using inelastic neutron spectroscopy. The high magnetic dilution removes the problematic molecular field discussed above (Fig. 1(c)) and suppresses the mixing between j_{eff} manifolds allowing us to consider a dominant response for Co^{2+} pairs. Probabilistic arguments can be used to illustrate this and is based on the observation that for a given random distribution of $x \text{Co}^{2+}$ and $(1-x) \text{Mg}^{2+}$ ions, the number of Co^{2+} pairs and the number of pairwise interactions for a given geometry present in the lattice far outweighs the number of Co^{2+} triplets and corresponding interactions between three Co^{2+} cations. For example, if there are N ways that a cluster with a particular geometry of 3 sites XYZ can occur in a given crystal, the relative probabilities of an arrangement of 3 Mg^{2+} , 1 Co^{2+} and 2 Mg^{2+} (and its permutations), 2 Co^{2+} and 1 Mg^{2+} (and its permutations) and 3 Co^{2+} occupying the three sites XYZ are $(1-x)^3$, $x(1-x)^2$, $x^2(1-x)$ and x^3 , respectively. Hence the ratio of numbers of spin pairs with XY , XZ and YZ geometry to spin triplets with XYZ geometry in the lattice is $= \frac{1-x}{x}$, and thus for small x , the number and hence inelastic neutron scattering intensities of Co^{2+} pair excitations far outweigh those from larger Co^{2+} clusters. We summarize the sample preparation and characterization techniques confirming the dominant pair response in this section and expanded description, including data from the techniques, of the characterization is provided in the Supplementary Information. We also discuss the neutron experiments applied to these materials.

Materials Preparation: Two polycrystalline samples of $\text{Co}_{0.03}\text{Mg}_{0.97}\text{O}$ were synthesized for this particular investigation. The first was synthesized by traditional solid state methods as outlined by Cowley *et al.*¹⁷. A second sample of $\text{Co}_{0.03}\text{Mg}_{0.97}\text{O}$ was made using solution techniques by mixing stoichiometric amounts of $\text{Mg}(\text{NO}_3)_2 \cdot 6\text{H}_2\text{O}$ and $\text{Co}(\text{NO}_3)_2 \cdot 6\text{H}_2\text{O}$. The solid mixture was dissolved in $\text{CH}_3\text{CH}_2\text{OH}$ and stirred for 1 h and heated to 70°C for 12 h yielding a pink gel. The gel was heated in air to 600°C with a heating rate of $20^\circ\text{C}/\text{h}$, reacted for 24 h, subsequently heated to 1000°C with a heating rate of $150^\circ\text{C}/\text{h}$, held for an additional 48 h and finally cooled to room temperature by switching off the furnace. Details concerning the synthesis and treatment of MgO and CoO samples are outlined by Cowley *et al.*¹⁷. We note that both magnetically substituted MgO samples gave consistent results and the comparison is shown in the Supplementary Information.

Laboratory X-ray Diffraction: Room temperature powder diffraction patterns of the end members (CoO and MgO) and $\text{Co}_x\text{Mg}_{1-x}\text{O}$ synthesized by sol-gel were collected over $2\theta = [25,100]^\circ$ in 0.02° steps on a Bruker D2 Phaser laboratory x-ray diffractometer utilizing a monochromated $\text{Cu K}\alpha_{1,2}$ source. As illustrated in the Supplementary Information, Rietveld refinement of $\text{Mg}_{1-x}\text{Co}_x\text{O}$ indicates that the solid solution assumes a rocksalt structure ($Fm\bar{3}m$) with a unit cell param-

eter $a = 4.2131(2)$ Å. Utilizing the measured values of the end members: CoO (4.2594(4) Å) and MgO (4.2118(1) Å), the unit cell parameter of 4.2131(2) Å corresponds to an $x = 0.025(5)$ according to Vegard's law³⁹, supporting that approximately 3% of the Mg^{2+} sites contain Co^{2+} .

Energy dispersive x-ray analysis: As a final direct confirmation of the concentration of Co^{2+} in our sample we performed energy dispersive x-ray measurements. Elemental analysis was performed using scanning electron microscopy (SEM) on a Hitachi SU-70 Schottky field emission gun SEM with an equipped Bruker Quantax energy dispersive X-ray detector. Energy dispersive X-ray spectroscopy (EDS) was carried out at 15 keV. The results are illustrated in Supplementary Information show the effect substitution and the homogeneous distribution of cobalt throughout the sample.

DC Magnetic Susceptibility: Temperature dependence of magnetization was measured on a Quantum Design MPMS for a 32.5 mg of polycrystalline $\text{Co}_{0.03}\text{Mg}_{0.97}\text{O}$ synthesized by sol-gel in an external DC field $\mu_0 H_{\text{ext}} = 0.1$ T. ZFC measurements were performed in 2 K steps spaced linearly from 2 K to 300 K, while FC measurements were performed in 5 K steps spaced linearly from 2 K to 170 K. For both ZFC/FC measurements. As described in the Supplementary Information, the Curie-Weiss constant was found to be consistent with pairs of Co^{2+} with an exchange interaction reported by Kanamori.¹⁶ The Curie constant was found to agree with a concentration of Co^{2+} ions consistent with starting concentrations, x-ray powder diffraction, and also EDX measurements. Susceptibility measurements therefore confirm the following key experimental properties of our substituted samples: the lack of magnetic ordering; the absence of measurable clustering of Co^{2+} evidenced from no measurable difference between zero-field and field-cooled sweeps; a Curie-Weiss constant consistent with a dominant 180° superexchange interaction; and finally a Curie constant consistent with starting concentrations.

Inelastic Neutron Scattering Details: 45.8 g, 45.2 g, 32.5 g and 15.7 g of $\text{Co}_{0.03}\text{Mg}_{0.97}\text{O}$ synthesized by the standard solid state and sol-gel methods, annealed MgO and CoO, respectively, were placed in separate airtight aluminum cans under helium. The high-energy measurements were made on the direct geometry MARI spectrometer. For measurements concerning the $\text{Co}_{0.03}\text{Mg}_{0.97}\text{O}$ sample synthesized by traditional solid state methods, MgO and CoO powders, the t_o chopper was operated at 50 Hz in parallel with a Gd chopper spun at frequencies $f = 350, 250$ and 150 Hz with incident energies $E_i = 30, 10$ and 5 meV, respectively, providing an elastic resolution of 0.7, 0.2 and 0.1 meV, respectively. For measurements concerning the $\text{Co}_{0.03}\text{Mg}_{0.97}\text{O}$ sample synthesized by sol-gel, the Gd chopper was spun at $f = 350$ Hz and 250 Hz with an E_i of 29.50 meV and 14.50 meV, providing an elastic resolution of 0.7 meV and 0.2 meV, respectively. For both $\text{Co}_{0.03}\text{Mg}_{0.97}\text{O}$ samples, a thick disk chopper with $f = 50$ Hz reduced the background from high-energy neutrons. A top loading Displex CCR cooled the samples to a base temperature of approximately 5 K. We note that further neutron inelastic scattering results comparing pure MgO, CoO, and our substituted MgO

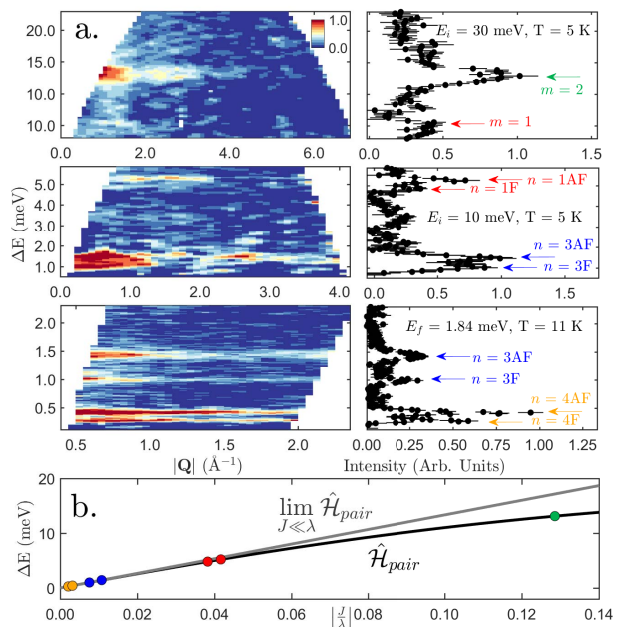


FIG. 2. (a) Background (using pure and non magnetic MgO) subtracted powder averaged neutron scattering intensity maps of $\text{Co}_{0.03}\text{Mg}_{0.97}\text{O}$ measured on (a, top left) MARI at 5 K with an $E_i = 30$ meV, (a, middle left) MARI at 5 K with an $E_i = 10$ meV and (a, bottom left) IRIS at 11 K with an $E_f = 1.84$ meV revealing 7 low energy bands of dispersionless magnetic excitations. The right column shows $|Q|$ -integrated cuts. Labels denote the coordination shell m and the type of coupling present with label n , both of which are determined in Fig. 3. (b) The black curve denotes the pair energy splitting as a function of the normalized exchange $\Delta E \left(\left| \frac{J}{\lambda} \right| \right)$. The points are measured energy positions from (a). The grey line is the same relationship derived using the projection theorem in the large λ limit^{19,20}.

sample are presented in the supplementary information.

For lower energies, measurements were made on the indirect geometry IRIS spectrometer. The final energy was fixed at 1.84 meV by PG002 analyzer crystals in near backscattering geometry. The graphite analyzers are cooled to reduce thermal diffuse scattering, providing an elastic resolution of 17.5 μeV . A combination of IRIS' long path length and its array of disc choppers, allowed us to select multiple time windows, resulting in the measured bandwidth being selectively increased to include energy transfers up to ~ 2 meV. A top loading dispex CCR was used to cool the sample to a base temperature of approximately 11 K. For all samples, identical instrumental and environmental parameters were employed on IRIS.

III. CO^{2+} PAIR INTERACTIONS:

Having discussed the materials preparation and characterization, we conclude that our rocksalt MgO sample substituted with Co^{2+} can be considered to be dominated by pairs of Co^{2+} ions. We now discuss the neutron scattering response of an isolated pair of magnetic ions and how it can be used to extract both the interaction distance and also the energy exchange interac-

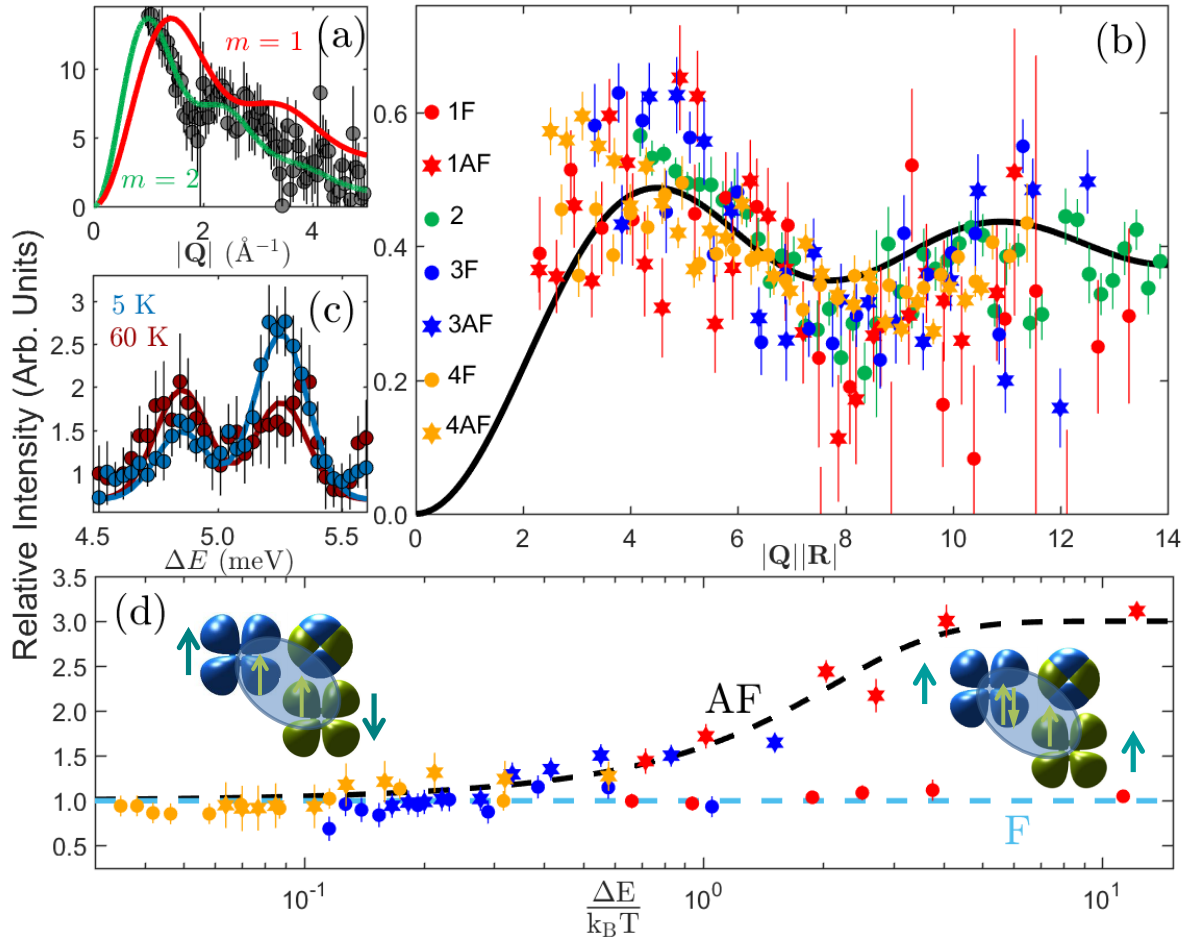


FIG. 3. (a) Constant- E cut ($\Delta E = [12,14]$ meV) from MARI at 5 K with an $E_i=30$ meV. The green curve is a fit to Eq. 5 with $|\mathbf{R}| = 4.2(3)$ Å ($m = 2$ pairs). The red curve is with $|\mathbf{R}|$ fixed as 2.98 Å ($m = 1$ pairs). (b) Scaled and form factor corrected $|\mathbf{Q}|$ -dependence of the intensities for all magnetic excitations with $|\mathbf{R}|$ calculated from the fitting routine described in (a). The solid black curve is $1 - \frac{\sin(|\mathbf{Q}||\mathbf{R}_n|)}{|\mathbf{Q}||\mathbf{R}_n|}$. (c) Constant- $|\mathbf{Q}|$ cut (MARI, $E_i=10$ meV) showing a different temperature dependence for the two peaks despite both being from $m = 1$ pairs. (d) Normalized temperature dependence of the Bose-factor corrected integrated intensity for all 7 excitations (Fig. 2) showing two universal curves calculated (dashed lines) for antiferromagnetic and ferromagnetic coupling. Both the integrated intensities and the calculated behaviour of antiferromagnetic or ferromagnetically coupled pairs were normalized by $I_F(T)$ as described in the main text. The inset is a pictorial representation of the sign of J as predicted by the GKA rules^{40–42} — antiferromagnetism (**left**) is a result of exchange between two half-filled t_{2g} orbitals while weaker ferromagnetism (**right**) is a result of exchange between a half-filled and completely filled t_{2g} orbitals. Yellow arrows denote local t_{2g} spin configurations and teal arrows denote total spin configurations on each Co^{2+} .

tion. By considering Co^{2+} pair interactions and only low energy excitations within the lowest $j_{\text{eff}} = \frac{1}{2}$ doublet (with $\hat{\mathbf{j}} = \beta\hat{\mathbf{S}}$), the interaction energy $\hat{\mathcal{H}}_{ex}$ between a pair of Co^{2+} ions in substituted $\text{Mg}_{0.97}\text{Co}_{0.03}\text{O}$, is approximated by

$$\hat{\mathcal{H}}'_{ex} = 2J\hat{\mathbf{S}}_1 \cdot \hat{\mathbf{S}}_2 \sim \tilde{\alpha}J \hat{\mathbf{j}}_1 \cdot \hat{\mathbf{j}}_2, \quad (3)$$

where $\hat{\mathbf{j}}$ and $\tilde{\alpha} = 2\beta^2$ denotes an effective total angular momentum operator with $j = \frac{1}{2}$ and a projection factor, respectively. As summarized by Fig. 1(b), the $\hat{\mathcal{H}}'_{ex}$ describes individual $j_{\text{eff}} = \frac{1}{2}$ pair excitations as transitions between triplet ($\Gamma_{\text{eff}} = 1$) and singlet ($\Gamma_{\text{eff}} = 0$) levels separated by an energy of $\Delta E = \tilde{\alpha}J$ ^{43–45}. The projection factor $\tilde{\alpha}$, in this low energy approximation, can be calculated by diagonalizing $\mathcal{H}_{S.I.} + \hat{\mathcal{H}}'_{ex}$ with

$\mathcal{H}_{\mathcal{M}\mathcal{F}} = 0$ owing to the lack of long range magnetic order in $\text{Co}_{0.03}\text{Mg}_{0.97}\text{O}$ ¹⁷. This is equivalent to the following Hamiltonian for two (labelled 1 and 2) interacting Co^{2+} ions,

$$\hat{\mathcal{H}}' = \tilde{\lambda}\tilde{\mathbf{l}}_1 \cdot \hat{\mathbf{S}}_1 + \tilde{\lambda}\tilde{\mathbf{l}}_2 \cdot \hat{\mathbf{S}}_2 + 2J\hat{\mathbf{S}}_1 \cdot \hat{\mathbf{S}}_2. \quad (4)$$

By considering $\tilde{l} = 1$ and $S = \frac{3}{2}$, this amounts to 144 basis states and a 144×144 matrix for this particular Hamiltonian in terms of the two particle basis of $|\tilde{l}_1, m_{\tilde{l}_1}, s_1, m_{s_1}\rangle \otimes |\tilde{l}_2, m_{\tilde{l}_2}, s_2, m_{s_2}\rangle$, where $\tilde{l}_i, m_{\tilde{l}_i}, s_i, m_{s_i}$ denote the eigenvalues corresponding to the $\tilde{\mathbf{l}}_i, \hat{\mathbf{l}}_{z,i}, \hat{\mathbf{S}}_i$ and $\hat{\mathbf{S}}_{z,i}$ operators, respectively, for the i^{th} particle. As illustrated in Fig. 2(b), in the limit of $J \ll \lambda$, $\Delta E(J)$ is linear with $\tilde{\alpha} = \frac{50}{9}$ in agreement with the projection theorem of angular momentum^{20,44}. Therefore, measur-

ing pair excitations with neutron spectroscopy provides a direct way to estimate the magnitude of exchange constant $|J|$ between neighboring Co^{2+} ions when this projection factor is taken into account. We note that this is independent of the sign of J and we discuss how that can be determined from the temperature dependence below.

While the excitation energy provides the magnitude $|J|$, the neutron spectroscopic momentum dependence can be used to extract the corresponding intra-pair distance \mathbf{R}_m , where m denotes the coordination shell. By applying the Hohenberg-Brinckman first moment sum rule and the single mode approximation for an isolated pair, excitations from a Co^{2+} pair have the following $|\mathbf{Q}|$ dependence^{43,50,51}

$$S(|\mathbf{Q}|) \propto \frac{|F(|\mathbf{Q}|)|^2}{\Delta E_o} \left(1 - \frac{\sin(|\mathbf{Q}||\mathbf{R}_m|)}{|\mathbf{Q}||\mathbf{R}_m|} \right), \quad (5)$$

with $|F(|\mathbf{Q}|)|^2$ the magnetic form factor. Since the modulation is solely dependent on the intra-pair distance \mathbf{R}_m , the excitation can be assigned to a particular pair and corresponding coordination shell in the $Fm\bar{3}m$ structure as illustrated in Fig. 1(a).

IV. RESULTS AND DISCUSSION:

Having discussed the theory for isolated pairs in dilute $\text{Co}_{0.03}\text{Mg}_{0.97}\text{O}$, we now present the experimental data. As illustrated by Fig. 2(a), low temperature/incident energy inelastic neutron spectroscopic measurements on powder $\text{Co}_{0.03}\text{Mg}_{0.97}\text{O}$ display a hierarchy of dispersionless excitations up to $\Delta E \sim 15$ meV. Based on the energy value of the excitations, we can assign an exchange constant as shown in Fig. 2(b) using the previously measured value for the spin-orbit coupling constant $\tilde{\lambda}$ ¹⁷ for isolated Co^{2+} on a rocksalt lattice. The intensities for each of the seven excitations in Fig. 2(a) exhibit a modulated $|\mathbf{Q}|$ -dependence, characteristic of pairwise interactions and thus distinguishing them from single-ion dispersionless crystal field excitations⁴³. As shown in Figs. 3(a,b), by fitting the intensity of each mode at different energies to Eq. 5, the different pair excitations could be assigned to relative coordination shells ranging from $m=1$ to $m=4$.

We now discuss the temperature dependence with the goal of extracting the sign of J . Antiferromagnetically coupled ($J > 0$) pairs of $j_{\text{eff}} = \frac{1}{2}$ spins consist of a singlet ground state and a triplet excited state while ferromagnetic coupling ($J < 0$) gives a triplet ground state and a single excited state. These two different coupling scenarios give distinct temperature dependences of the integrated intensity that scales as the thermal population difference between the ground and excited states^{51,52}, with antiferromagnetic pairs following

$$I_{AF}(T) \propto (1 - e^{-\Delta E/k_B T}) / (1 + 3e^{-\Delta E/k_B T}) \quad (6)$$

and ferromagnetic pairs

$$I_F(T) \propto (1 - e^{-\Delta E/k_B T}) / (3 + e^{-\Delta E/k_B T}), \quad (7)$$

such that as $T \rightarrow 0$ K, the ratio

$$\frac{I_{AF}}{I_F} = \frac{3 + e^{-\Delta E/k_B T}}{1 + 3e^{-\Delta E/k_B T}} \rightarrow 3. \quad (8)$$

As illustrated in Fig. 3(d), by normalizing the temperature dependence by $I_F(T)$, all integrated intensities fall onto either one of two universal curves describing antiferromagnetism or ferromagnetism.

All extracted values of J based on the energy, momentum, and temperature dependence discussed above are summarized in Tab. I. All coordination shells, with the exception of $m = 2$, display two closely spaced excitations with differing signs for the exchange constant as illustrated in Fig. 3(c) for the ~ 5 meV excitation. This presence of dual ferro and antiferromagnetic interactions for $m = 1, 3$ and 4 is consistent with the GKA rules^{40-42,53} since each of these exchange pathways, consists of at least one 90° Co^{2+} - Co^{2+} interaction involving the overlap of half and filled orbitals. Indeed, the GKA rules predict that the combination of the orbital degree of freedom for *each* Co^{2+} and a lack of orbital ordering (or anisotropy) would manifest itself as either a direct antiferromagnetic $t_{2g}^1-t_{2g}^1$ or a weaker ferromagnetic $t_{2g}^1-t_{2g}^2$ exchange interaction. As summarized in Fig. 3(d) and Tab. I, the experimental results verify the GKA rules^{40-42,53} as the antiferromagnetic interaction is stronger than the ferromagnetic alternative for all the $m \neq 2$ excitations while the 180° Co^{2+} - O^{2-} - Co^{2+} $m = 2$ coupling leads to only a strong antiferromagnetic interaction.

Having assigned the signs of the 7 exchange constants for dilute $\text{Co}_{0.03}\text{Mg}_{0.97}\text{O}$, we now provide a comparison with thermodynamic data and previously measured and calculated exchange constants for bulk CoO. The additional complication of a dual ferro and antiferromagnetic interactions for most m exchange pathways in combination to the entanglement of individual spin-orbit manifolds in the presence of magnetic order provides a possible explanation for the large range of J values reported for CoO^{16,30,31,35,54-58}. As summarized in Tab. I, the values of J show good agreement with three general trends reported by experiment³⁰: (i) dominant $J_2 > 0$, (ii) a $J_1 < 0$ and (iii) a significantly smaller but non-negligible J_3 , all in broad agreement with the trends concluded from a recent $GGA + U$ DFT calculation on CoO (though no such dual exchange was predicted)³². In terms of thermodynamic data, the Curie-Weiss constant is related to the exchange interactions *via* $\Theta_{CW} = -\frac{2}{3}S(S+1)\sum_i z_i J_i$, where the spin value $S = \frac{3}{2}$ and z_i is the number of neighbors for each i^{th} exchange interaction^{48,49}. Following Kanamori¹⁶ and applying a correction for spin-orbit coupling, the effective Curie-Weiss temperature $\tilde{\theta}_{CW}$ is listed in Tab. I and compared against a mean field T_N calculated based just on J_2 . The estimated $\tilde{\theta}_{CW}$ of $-295(5)$ K ($-25.4(5)$ meV) and a mean-field estimate of T_N of $283(5)$ K ($24.4(3)$ meV), demonstrate close similarities with experimentally determined values of $\theta_{CW} = -330(4)$ K^{46,47} and $T_N = 291(4)$ K²⁵, respectively, for CoO. The excellent agreement results from the near perfect cancellation of antiferromagnetic and ferromagnetic interactions for all coordinations with the exception of $m = 2$ (the 180° interaction). Although the $\text{Co}_{0.03}\text{Mg}_{0.97}\text{O}$ lattice ($a = 4.21$ Å) is contracted rela-

TABLE I. Magnetic exchange constants for $\text{Co}_{0.03}\text{Mg}_{0.97}\text{O}$ determined by the current study, magnetic exchange constants for CoO as cited in literature^{30,31} and calculated for CoO by Deng *et al.*³² using $GGA + U$ DFT. The values from $GGA + U$ DFT have been renormalized such that J_2 is equal to the value from this current study. The values of T_N , θ_{CW} and λ reported in literature^{17,25,46,47} for CoO have been included for the purposes of a comparison to the mean field value^{48,49} of θ_{CW} corresponding to the J values determined by the current study.

Quantity / Source	Current Study (meV)	Literature Studies (meV)	Calculated (meV) ³²
λ		24(5) ¹⁷	
J_{1AF}	1.000(8)	0.60 to -0.31 ^{16,30}	-0.97(2)
J_{1F}	-0.918(6)		
J_2 or J_{2AF}	3.09(5)	2.8 to 0.0013 ³⁰	3.09(5)
J_{3AF}	0.258(1)	-0.67 ³¹	-0.461(8)
J_{3F}	-0.182(1)		
J_{4AF}	0.0759(4)		-0.0085(1)
J_{4F}	-0.0504(4)		
T_N	24.4(3) ^a	25.1(4) ²⁵	
θ_{CW}	-25.4(5)	-28.4(4) ^{46,47}	

^a Calculated using the mean field estimate $T_N \sim \left| \frac{2}{3} S(S+1) z_2 J_2 \right|$

tive to that of pure CoO ($a = 4.26 \text{ \AA}$ ⁵⁹), the above agreements of energy scale are highly suggestive that the Co^{2+} - Co^{2+} exchange interactions are not greatly changed, or at least any changes are smaller than systematic errors introduced by attempting to simplify the scheme in pure CoO. Hence the present results represent a comprehensive set of interaction energy estimates for CoO.

In summary, we have disentangled the exchange and spin-orbit interactions for Co^{2+} on a rocksalt lattice. Through a combined analysis of the energy, momentum, and temperature dependence, we have extracted 7 exchange constants out to four coordination shells. Both ferro and antiferromagnetic interactions are ob-

served with the exception of second neighbor interactions through linear Co^{2+} - O^{2-} - Co^{2+} bridges, in agreement with both the GKA rules and thermodynamic data. The results demonstrate that in the case of an orbital degeneracy in the t_{2g} channel dual ferro and antiferromagnetic interactions occur with comparable magnitudes.

We acknowledge useful conversations with T. Guidi, J. R. Stewart, M. A. Green, T. J. Williams, K. H. Hong, G. M. McNally and S. E. Maytham. We are grateful to the Carnegie Trust for the Universities of Scotland, the Royal Society, the STFC, the ERC and the EPSRC for financial support. P.M.S. acknowledges financial support from the CCSF and the University of Edinburgh through the GRS and PCDS.

[†] Deceased 27 January 2015

¹ Y. Tokura and N. Nagaosa, *Science* **288**, 462 (2000).

² E. Dagotto, *Science* **309**, 257 (2005).

³ K. I. Kugel and D. I. Khomskii, *Phys. Usp.* **136**, 621 (1982).

⁴ Y. Okamoto, M. Nohara, H. A. Katori, and H. Takagi, *Phys. Rev. Lett.* **99**, 137207 (2007).

⁵ R. Wang, A. Go, and A. J. Millis, *Phys. Rev. B* **95**, 045133 (2017).

⁶ G. Jackeli and G. Khaliullin, *Phys. Rev. Lett.* **102**, 017205 (2009).

⁷ C. G. Shull, W. A. Strauser, and E. O. Wollan, *Phys. Rev.* **83**, 333 (1951).

⁸ Y. Y. Li, *Phys. Rev.* **100**, 627 (1955).

⁹ W. L. Roth, *Phys. Rev.* **110**, 1333 (1958).

¹⁰ B. van Laar, *Phys. Rev.* **138**, A584 (1965).

¹¹ S. K. Satija, J. D. Axe, G. Shirane, H. Yoshizawa, and K. Hirakawa, *Phys. Rev. B* **21**, 2001 (1980).

¹² A. M. Oles, P. Horsch, L. F. Feiner, and G. Khaliullin, *Phys. Rev. Lett.* **96**, 147205 (2006).

¹³ M. W. Haverkort, A. Tanaka, L. H. Tjeng, and G. A. Sawatzky, *Physical Rev. Lett.* **99**, 257401 (2007).

¹⁴ B. C. Larson, W. Ku, J. Z. Tischler, C.-C. Lee, O. D. Restrepo, A. G. Eguiluz, P. Zschack, and K. D. Finkelstein, *Phys. Rev. Lett.* **99**, 026401 (2007).

¹⁵ J. Sakurai, W. J. L. Buyers, R. A. Cowley, and

G. Dolling, *Phys. Rev.* **167**, 510 (1968).

¹⁶ J. Kanamori, *Progr. Theor. Phys.* **17**, 177 (1957).

¹⁷ R. A. Cowley, W. J. L. Buyers, C. Stock, Z. Yamani, C. Frost, J. W. Taylor, and D. Prabhakaran, *Phys. Rev. B* **88**, 205117 (2013).

¹⁸ F. Wallington, A. M. Arévalo-Lopez, J. W. Taylor, J. R. Stewart, V. García-Sakai, J. P. Attfield, and C. Stock, *Phys. Rev. B* **92**, 125116 (2015).

¹⁹ D. I. Khomskii, *Transition Metal Compounds* (Cambridge University Press, 2014).

²⁰ A. Abragam and B. Bleaney, *Electron paramagnetic resonance of transition ions* (OUP Oxford, 2012).

²¹ J. Kanamori, *Progr. Theor. Phys.* **17**, 197 (1957).

²² W. J. L. Buyers, T. M. Holden, E. C. Svensson, R. A. Cowley, and M. T. Hutchings, *J. Phys. C Solid State Phys.* **4**, 2139 (1971).

²³ W. J. L. Buyers, T. M. Holden, E. C. Svensson, and D. J. Lockwood, *Phys. Rev. B* **30**, 6521 (1984).

²⁴ R. A. Cowley, W. J. L. Buyers, P. Martel, and R. W. H. Stevenson, *J. Phys. C Solid State Phys.* **6**, 2997 (1973).

²⁵ W. Jauch, M. Reehuis, H. J. Bleif, F. Kubanek, and P. Pattison, *Phys. Rev. B* **64**, 052102 (2001).

²⁶ R. Coldea, D. A. Tennant, E. M. Wheeler, E. Wawrzynska, D. Prabhakaran, M. Telling, K. Habicht, P. Smeibidl, and K. Kiefer, *Science* **327**, 177 (2010).

²⁷ B. Grenier, S. Petit, V. Simonet, E. Canévet, L.-P. Reg-

- nault, S. Raymond, B. Canals, C. Berthier, and P. Lejay, *Phys. Rev. Lett.* **114**, 017201 (2015).
- ²⁸ H. D. Zhou, C. Xu, A. M. Hallas, H. J. Silverstein, C. R. Wiebe, I. Umegaki, J. Q. Yan, T. P. Murphy, J.-H. Park, Y. Qiu, J. R. D. Copley, J. S. Gardner, and Y. Takano, *Phys. Rev. Lett.* **109**, 267206 (2012).
- ²⁹ A. L. Dalverny, J. S. Filhol, F. Lemoigno, and M. L. Doublet, *J. Phys. Chem. C* **114**, 21750 (2010).
- ³⁰ M. Feyngenson, X. Teng, S. E. Inderhees, Y. Yiu, W. Du, W. Han, J. Wen, Z. Xu, A. A. Podlesnyak, J. L. Niedziela, M. Hagen, Y. Qiu, C. M. Brown, L. Zhang, and M. C. Aronson, *Phys. Rev. B* **83**, 174414 (2011).
- ³¹ K. Tomiyasu and S. Itoh, *J. Phys. Soc. Jpn.* **75**, 084708 (2006).
- ³² H.-X. Deng, J. Li, S.-S. Li, J.-B. Xia, A. Walsh, and S.-H. Wei, *Appl. Phys. Lett.* **96**, 162508 (2010).
- ³³ Z. Yamani, W. J. L. Buyers, R. A. Cowley, and D. Prabhakaran, *Can. J. Phys.* **88**, 729 (2010).
- ³⁴ G. Fischer, M. Däne, A. Ernst, P. Bruno, M. Lüeders, Z. Szotek, W. Temmerman, and W. Hergert, *Phys. Rev. B* **80**, 014408 (2009).
- ³⁵ C. Kant, T. Rudolf, F. Schrettle, F. Mayr, J. Deisenhofer, P. Lunkenheimer, M. V. Eremin, and A. Loidl, *Phys. Rev. B* **78**, 245103 (2008).
- ³⁶ See Supplemental Material at [URL to be inserted by publisher] for a description of sample characterization.
- ³⁷ A. Furrer, A. Podlesnyak, and K. W. Krämer, *Phys. Rev. B* **92**, 104415 (2015).
- ³⁸ E. C. Svensson, M. Harvey, W. J. L. Buyers, and T. M. Holden, *J. Appl. Phys.* **49**, 2150 (1978).
- ³⁹ L. Vegard, *Z. Phys.* **5**, 17 (1921).
- ⁴⁰ J. B. Goodenough, *J. Phys. Chem. Solids* **6**, 287 (1958).
- ⁴¹ J. Kanamori, *J. Phys. Chem. Solids* **10**, 87 (1959).
- ⁴² P. W. Anderson, *Phys. Rev.* **79**, 350 (1950).
- ⁴³ J. T. Haraldsen, T. Barnes, and J. L. Musfeldt, *Phys. Rev. B* **71**, 064403 (2005).
- ⁴⁴ M. Rose, *Elementary Theory of Angular Momentum*, Dover Books on Physics and Chemistry (Dover, 1995).
- ⁴⁵ A. Furrer and O. Waldmann, *Rev. Mod. Phys.* **85**, 367 (2013).
- ⁴⁶ T. Nagamiya, K. Yosida, and R. F. Kubo, *Adv. Phys.* **4**, 1 (1955).
- ⁴⁷ J. R. Singer, *Phys. Rev.* **104**, 929 (1956).
- ⁴⁸ K. Lee, J. Lee, C. Lee, and M. Whangbo, *Bull. Korean Chem. Soc.* **35**, 1277 (2014).
- ⁴⁹ C. Kittel, *Introduction to solid state physics* (Wiley, New York, 2005).
- ⁵⁰ P. C. Hohenberg and W. F. Brinkman, *Phys. Rev. B* **10**, 128 (1974).
- ⁵¹ M. B. Stone, M. D. Lumsden, S. Chang, E. C. Samulon, C. D. Batista, and I. R. Fisher, *Phys. Rev. Lett.* **100**, 237201 (2008).
- ⁵² Y. Zhu, *Modern techniques for characterizing magnetic materials* (Springer Science & Business Media, 2005).
- ⁵³ J. B. Goodenough, *Phys. Rev.* **100**, 564 (1955).
- ⁵⁴ M. Tachiki, *J. Phys. Soc. Jpn.* **19**, 454 (1964).
- ⁵⁵ M. El-Batanouny, *J. Phys.: Condens. Matter* **14**, 6281 (2002).
- ⁵⁶ H.-h. Chou and H. Y. Fan, *Phys. Rev. B* **13**, 3924 (1976).
- ⁵⁷ R. R. Hayes and C. H. Perry, *Solid State Commun.* **13**, 1915 (1973).
- ⁵⁸ T. Satoh, R. Iida, T. Higuchi, Y. Fujii, A. Koreeda, H. Ueda, T. Shimura, K. Kuroda, V. I. Butrim, and B. A. Ivanov, *Nat. Commun.* **8**, 638 (2017).
- ⁵⁹ S. Sasaki, K. Fujino, and Y. TakÉchi, *Proc. Jpn. Acad. Ser. B Phys. Biol. Sci.* **55**, 43 (1979).

Supplementary information for “Disentangling orbital and spin exchange interactions for Co^{2+} on a rocksalt lattice”

P. M. Sarte,^{1,2} R. A. Cowley,^{3,†} E. E. Rodriguez,⁴ E. Pachoud,^{1,2} D. Le,⁵ V. García-Sakai,⁵ J. W. Taylor,⁵ C. D. Frost,⁵ D. Prabhakaran,³ C. MacEwen,⁶ A. Kitada,⁷ A. J. Browne,^{1,2} M. Songvilay,^{2,6} Z. Yamani,⁸ W. J. L. Buyers,^{8,9} J. P. Attfield,^{1,2} and C. Stock^{2,6}

¹*School of Chemistry, University of Edinburgh, Edinburgh EH9 3FJ, United Kingdom*

²*Centre for Science at Extreme Conditions, University of Edinburgh, Edinburgh EH9 3FD, United Kingdom*

³*Department of Physics, Clarendon Laboratory, University of Oxford, Park Road, Oxford, OX1 3PU, United Kingdom*

⁴*Department of Chemistry and Biochemistry, University of Maryland, College Park, Maryland 20742, USA*

⁵*ISIS Facility, Rutherford Appleton Laboratory, Chilton, Didcot OX11 0QX, United Kingdom*

⁶*School of Physics and Astronomy, University of Edinburgh, Edinburgh EH9 3FD, United Kingdom*

⁷*Department of Materials Science and Engineering,*

Kyoto University, Yoshida-honmachi, Sakyo, Kyoto 606-8501, Japan

⁸*National Research Council, Chalk River, Ontario K0J 1J0, Canada*

⁹*Canadian Institute of Advanced Research, Toronto, Ontario M5G 1Z8, Canada*

(Dated: August 24, 2018)

Supplementary information is provided on sample characterization of the MgO powders weakly substituted with magnetic Co^{2+} . The purpose of this characterization is to determine the Co^{2+} concentration and to show the lack of observable Co^{2+} clustering therefore implying a homogenous distribution of magnetic ions on the rocksalt MgO lattice in our samples. Details on the estimation of the Curie-Weiss temperature used in the main text to compare our results to pure CoO is also given.

I. DIFFRACTION

X-ray diffraction results are shown in Fig. S1 (a) for pure CoO and MgO and our diluted sample of $\text{Mg}_{1-x}\text{Co}_x\text{O}$. Rietveld refinement of $\text{Mg}_{1-x}\text{Co}_x\text{O}$ indicates that the solid solution assumes a rocksalt structure ($Fm\bar{3}m$) with a unit cell parameter $a = 4.2131(2)$ Å. Utilizing the measured values of the end members: CoO (4.2594(4) Å) and MgO (4.2118(1) Å), the unit cell parameter of 4.2131(2) Å corresponds to an $x = 0.025(5)$ according to Vegard’s law³, confirming that approximately 3% of the Mg^{2+} sites contain Co^{2+} .

II. SUSCEPTIBILITY

Concentration: For the purposes of consistency, the value of x was also determined *via* DC magnetic susceptibility. As illustrated in Fig. S1(b), there is a distinct absence of magnetic ordering between 2 and 300 K, in contrast to CoO. The high temperature portion of the data ($T = [200, 300]$ K) exhibits Curie-Weiss behavior with a Curie constant C and Curie-Weiss temperature θ_{CW} of 0.105(8) emu · K/mol $\text{Mg}_{0.97}\text{Co}_{0.03}\text{O}$ and $-41(6)$ K, respectively. As established in the mean field derivation of the Curie-Weiss law, the Curie constant C must account for all Co^{2+} in $\text{Co}_x\text{Mg}_{1-x}\text{O}$ and thus its value is directly proportional to x .

Recall that the effective paramagnetic moment is defined as

$$\mu_{eff} = g_J \cdot \sqrt{S \cdot (S + 1)}, \quad (1)$$

where g_J is the Landé g-factor equal to 2 and $S = \frac{3}{2}$. This would give an expected magnetic moment for Co^{2+} of $\mu_{eff} = 3.9\mu_B$.

In order to compare the expected value of μ_{eff} in Eq. 1 to the its experimentally determined value, one must first

employ the definition of the Curie constant

$$C = \frac{N\mu_{eff}^2}{3k_B}. \quad (2)$$

It should be noted that χ in Fig. S1(b) was normalized by moles and thus N in Eq. 2 must be set to N_A . Finally, by solving for μ_{eff} , inserting the value of 0.105(8) emu/K mol $\text{Mg}_{0.97}\text{Co}_{0.03}\text{O}$, and utilizing the fact that only 3% of the Co^{2+} sites are in fact magnetic one obtains an effective paramagnetic moment of

$$\mu_{eff} = \sqrt{\frac{3k_B}{N_A} \cdot \frac{1}{0.03} \cdot 0.105(8)} = 5.3 \pm 1.2 \mu_B, \quad (3)$$

in agreement with the predicted value (Eq. 1) and thus confirming that approximately 3% of the Co^{2+} sites contain Co^{2+} . This is consistent with the starting concentration and also the values estimated from x-ray diffraction discussed above. The large estimated errorbar in the above equation results from the error in the Co^{2+} concentration and also the mass of the measured sample.

Homogeneous concentration of Co^{2+} : A confirmation of the prevalence of pairs over larger clusters of Co^{2+} , and hence a homogeneous distribution of Co^{2+} in the sample, is given the value of the experimentally determined Curie-Weiss constant from DC susceptibility shown in Fig. S1 (b). It is rationalized based on probability that Co^{2+} in $\text{Mg}_{0.97}\text{Co}_{0.03}\text{O}$ are predominately isolated (i.e. single ions), while a smaller but significant amount of Co^{2+} exhibit pairwise interactions. These pairs are coupled by J_i where the index i denotes a particular coordination shell. A confirmation of the presence of pairs can be obtained from Curie-Weiss temperature which in the mean-field limit has the form,

$$\theta_{CW} = -\frac{2S(S+1) \sum_i z_i J_i}{3}, \quad (4)$$

where z_i denotes the number of atoms/ions coupled to the central atom/ion with magnetic constant J_i ⁶. The

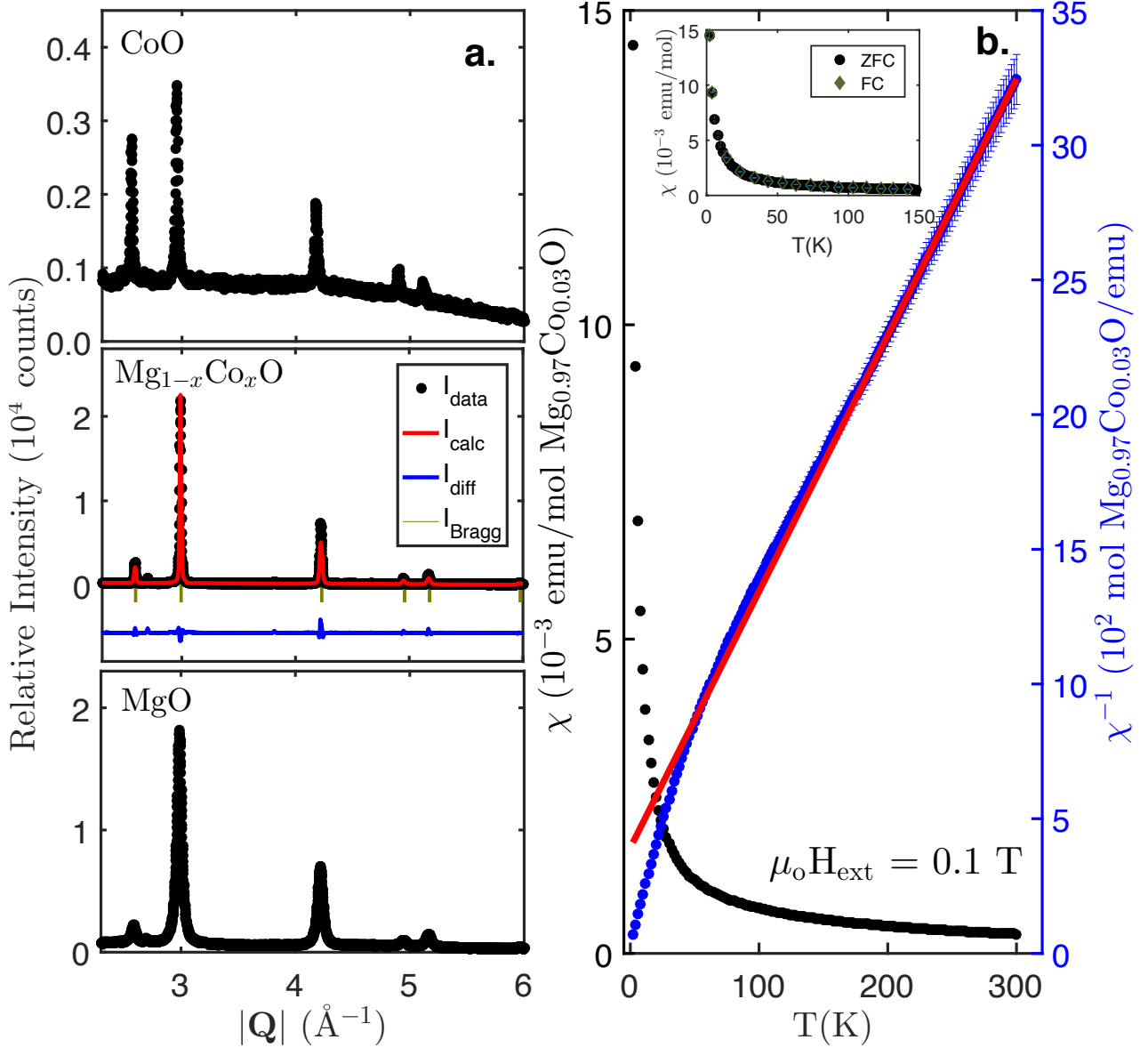


Figure S1. (a) Room temperature diffraction profiles for CoO, $Mg_{1-x}Co_xO$ and MgO collected on a Bruker D2 Phaser x-ray diffractometer utilizing a monochromated Cu $K_{\alpha,1,2}$ source. Rietveld refinement ($\chi^2 = 6.91$, $R_p = 10.12\%$ and $R_{wp} = 13.25\%$) of $Co_xMg_{1-x}O$ indicates that the solid solution assumes a rock-salt structure ($Fm\bar{3}m$) with a unit cell parameter $a = 4.2131(2)$ \AA , corresponding to an $x = 0.025(5)$ according to Vegard's law³. (b) Temperature dependence of molar magnetic susceptibility ($\mu_0 H_{\text{ext}} = 0.1$ T) and its inverse for polycrystalline $Co_xMg_{1-x}O$ synthesized by sol-gel. ZFC measurements were performed in 2 K steps spaced linearly from 2 K to 300 K, whilst FC measurements were performed in 5 K steps spaced linearly. (inset) A comparison of the temperature dependence of FC and ZFC molar magnetic susceptibility reveals no significant difference indicating an absence of measurable glassy behavior. The high temperature portion of the data ($T = [200,300]$ K) exhibits Curie-Weiss behavior (red-line) with a Curie constant C and Curie-Weiss temperature θ_{CW} of $0.105(8)$ emu \cdot K/mol $Co_{0.03}Mg_{0.97}O$ and $-41(6)$ K, respectively.

concurrent presence of AFM and FM behavior in each coordination shell, with the exception of the second, implies that θ_{CW} would be dominated by the second coordination shell. Before proceeding, it is worth noting that Kanamori⁷ utilizing second order perturbation theory deduced that strong spin-orbit coupling in CoO substantially reduces the Curie-Weiss temperature estimated by the mean field approximation in Eq. 4. Utilizing a value of approximately 0.9 eV for the energy splitting between the 4F and 4P free ion states, Kanamori derived that his

mean field estimate of $\theta_{CW} \sim -530$ K was overestimated by a factor of 1.9 if spin-orbit coupling was neglected. Thus, by inserting the values of $S = \frac{3}{2}$, $J_2 = 35.9(6)$ K (3.09(5) meV), setting the value of z as 1 since individual Co^{2+} pairwise interactions are of interest and dividing by a correction factor of 1.9 deduced by Kanamori⁷ to

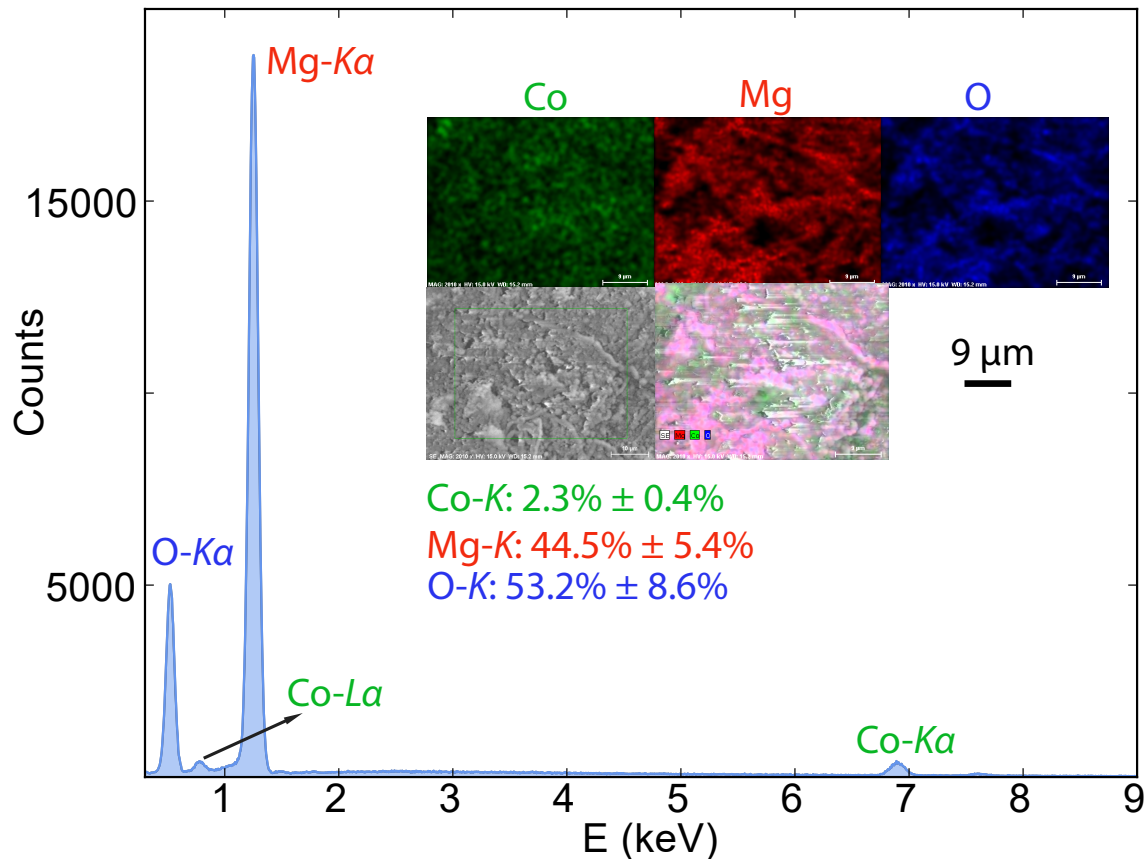


Figure S2. Energy dispersive spectroscopy analysis of the substituted MgO sample used in our neutron experiments. The resulting elemental analysis is shown and consistent with x-ray and susceptibility measurements.

account for spin-orbit coupling yields a value of

$$\tilde{\theta}_{CW} = -\frac{2 \cdot \frac{3}{2}(\frac{3}{2} + 1) \cdot (1)(35.9(6))}{3 \cdot 1.9} = -44.9(7) \text{ K}, \quad (5)$$

in excellent agreement with the experimentally determined value of $-41(6)$ K for our dilute samples shown in Fig. S1 (b). The success in accounting for the Curie-Weiss temperature implies that the cooperative magnetism of $\text{Mg}_{0.97}\text{Co}_{0.03}\text{O}$ can be approximated as being attributed to Co^{2+} pairwise interactions exclusively. As a concluding comment, it is worthwhile to note that the magnetic susceptibility exhibits no difference between ZFC/FC, implying an absence of glassy behavior down to 2 K. This absence of glassy behavior supports our claim that larger molecular clusters are absent since these would be expected to yield glassy behavior and thus a ZFC/FC split.

III. ENERGY DISPERSIVE X-RAY ANALYSIS:

Energy dispersive x-ray analysis results are displayed in Fig. S2. As illustrated in the figures, the concentration of magnetic Co^{2+} was measured to be $2.3\% \pm 0.4\%$, consistent with susceptibility and diffraction results

discussed above. The inset figures to Fig. S2 also show the distribution to be uniform with no obvious clustering consistent with our susceptibility analysis above.

IV. SPECTROSCOPIC COMPARISON OF PURE AND SUBSTITUTED SAMPLES

We compare the spectroscopic response of pure CoO, MgO, and our two dilute samples prepared with solid state and solution techniques in Fig. S3. The two different sample preparation techniques provide consistent spectroscopic results for all energy transfers measured. The results are different from those obtained in pure CoO and MgO indicative of a lack of local large clusters of Co^{2+} magnetic moments. Based on this comparison, we conclude that the results presented in this paper are independent of sample preparation techniques and also that our samples do not contain local regions of magnetic clustering.

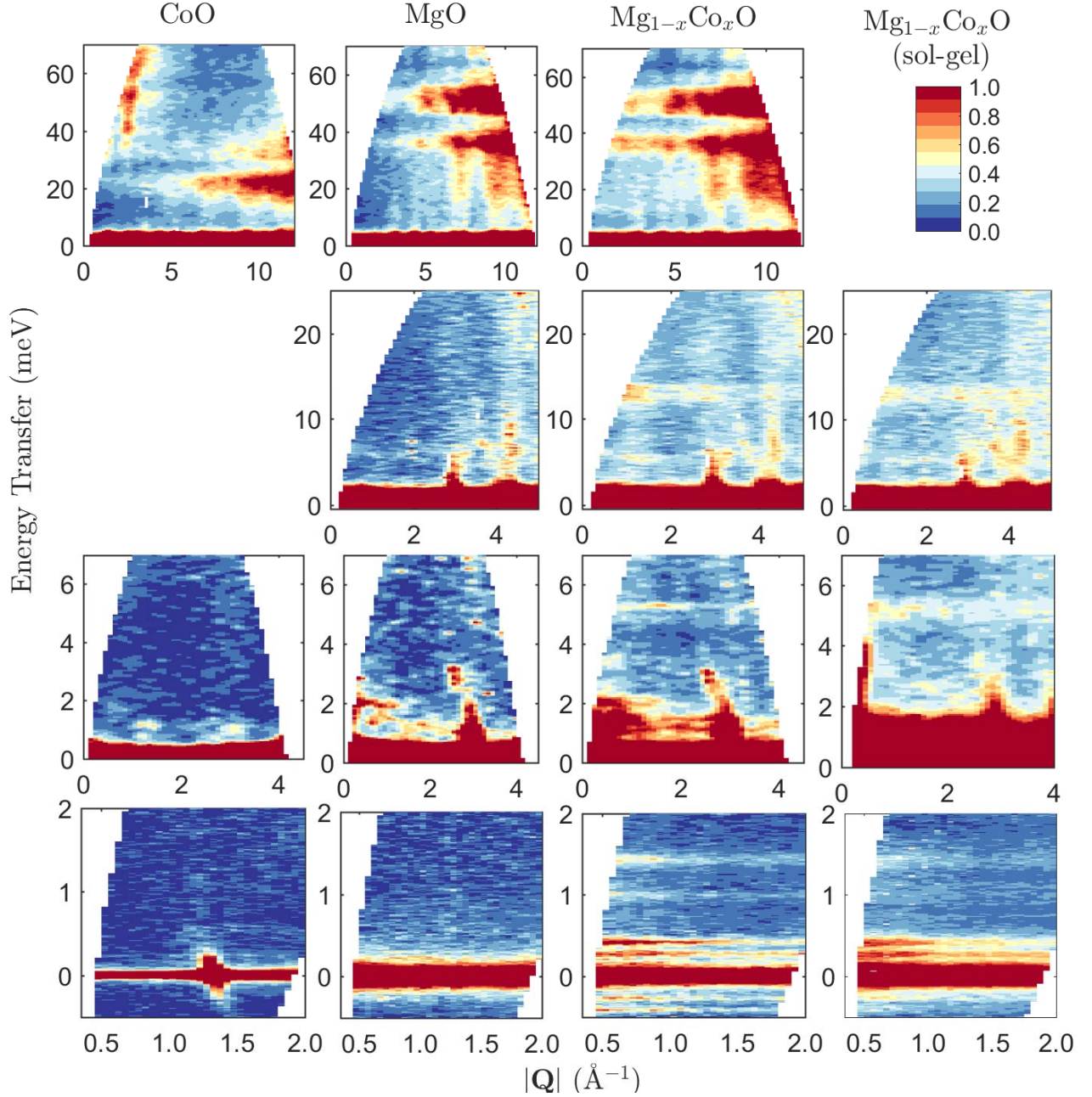


Figure S3. A comparison of raw (non-background subtracted) $I(|\mathbf{Q}|, E)$ maps at 5 K for CoO, MgO, $\text{Mg}_{0.97}\text{Co}_{0.03}\text{O}$ synthesized by standard solid state methods and $\text{Mg}_{0.97}\text{Co}_{0.03}\text{O}$ synthesized by sol-gel. Each column corresponds to a particular compound as labelled from above. Rows 1 to 3 correspond to incident energies of 85 meV ($f = 300$ Hz), 30 meV ($f = 350$ Hz), 10 meV ($f = 250$ Hz) measured on MARI, respectively, whilst row 4 corresponds to a final energy of 1.84 meV measured on IRIS. Three exceptions include: CoO in row 1 corresponding to an incident energy of 100 meV ($f = 350$ Hz), $\text{Mg}_{0.97}\text{Co}_{0.03}\text{O}$ (sol-gel) in rows 2 and 3 correspond to incident energies of 29.5 meV ($f = 350$ Hz) and 14.5 meV ($f = 250$ Hz), respectively. All $I(|\mathbf{Q}|, E)$ maps have been renormalized to a common scale.

V. TABULATED EXPERIMENTAL ENERGY POSITIONS:

In this section we list the measured experimental energy positions and the calculated coordination shell (m) along with the calculated J including the sign indicative of ferromagnetic or antiferromagnetic coupling. The results are used below for the analysis of the Curie-Weiss constant.

VI. ESTIMATION OF THE CURIE-WEISS TEMPERATURE FOR COO VIA A MEAN FIELD APPROACH:

The interpretation of the magnetic excitations illustrated in Fig. 2(a) in the main text as distinct pairwise interactions due to the assumption of physical homogeneity in $\text{Co}_{0.03}\text{Mg}_{0.97}\text{O}$ corresponds to a direct analog of the physical model underlying the mean field estimate of the Curie-Weiss temperature given by Eq. 4. Before θ_{CW} can

TABLE I. Tabular summary of the calculated parameters related energy peak position to exchange constant

Experimental ΔE_o (meV)	Calculated $ \mathbf{R} $ (Å)	Relative Coordination Shell m	Type of Coupling	Calculated J (meV)
13.1(2)	4.2(3)	2	AF	3.09(5)
5.256(4)	4.1(5)	1	AF	1.000(8)
4.857(3)	4.4(3)	1	F	-0.918(6)
1.434(3)	5.5(5)	3	AF	0.258(1)
0.998(4)	5.4(6)	3	F	-0.182(1)
0.420(2)	6.3(7)	4	AF	0.0759(4)
0.279(2)	5.8(5)	4	F	-0.0504(4)

TABLE II. Select summary of crystallographic parameters of $\text{Co}_{0.03}\text{Mg}_{0.97}\text{O}$. The number of neighbors in a relative coordination shell m was determined assuming a collinear type-II antiferromagnetic structure possessed by $\text{CoO}^{11,12}$.

Relative Coordination Shell m	Distance at 298 K $ \mathbf{R}_m $ (Å)	Number of Neighbors in m	AF Coupling	F Coupling
1	2.983(1)	12	6	6
2	4.218(2)	6	6	0
3	5.166(2)	24	12	12
4	5.966(2)	12	0	12

be estimated with Eq. 4, it is important to note that while the value of $S = \frac{3}{2}$ is well-established as determined by Hund's rules^{4,8-10}, the value of z_i possesses an inherent ambiguity in $\text{Co}_{0.03}\text{Mg}_{0.97}\text{O}$. Since $\text{Co}_{0.03}\text{Mg}_{0.97}\text{O}$ itself does not magnetically order down to 2 K⁸ as illustrated in Fig. S1, the number of Co^{2+} exhibiting each type of coupling J_i as measured by inelastic neutron spectroscopy cannot be determined directly by referring to its magnetic structure.

We have assumed that the interactions in $\text{Co}_{0.03}\text{Mg}_{0.97}\text{O}$ are approximately analogous to those in CoO . Utilizing the assumption of the equivalence between $\text{Co}_{0.03}\text{Mg}_{0.97}\text{O}$ and CoO , the values of z_i can be determined by investigating the number of couplings between different coordination shells in the collinear type-II antiferromagnetic structure proposed for $\text{CoO}^{11,12}$. The determination of the value of z_i for coordination shells $m = 1 \dots 4$ was accomplished by first applying a transformation of the cubic $Fm\bar{3}m$ space group into its rhombohedral maximal subgroup $R\bar{3}m$ of the hexagonal crystal family. This transformation results in the stacking of the $\langle 111 \rangle$ planes along c in the $R\bar{3}m$ representation. Since Co^{2+} in $0, \pm 2, \dots$ and $\pm 1, \pm 3, \dots$ layers relative the $\langle 111 \rangle$ layer of reference are coupled F and AF, respectively in a collinear type-II

antiferromagnet, then the c coordinate of each Co^{2+} in a particular m coordination shell determined the type of coupling each Co^{2+} was predicted to exhibit. It should be noted that this analysis suggests only ferromagnetic correlations should exist in $m = 4$ coordination shell, in contradiction with the AF assignment to the magnetic excitation at $\Delta E_o = 0.0759(2)$ meV, which may indicate the presence of magnetic frustration. The number of Co^{2+} in each coordination shell exhibiting F or AF coupling is summarized in Tab. II.

By inserting the values of S as determined from Hund's rules, J_i as determined from the measured energy transfers and z_i as determined from the aforementioned rhombohedral transformation analysis, into the mean field estimate of the Curie-Weiss temperature with Kanamori's second perturbation order corrections, one obtains

$$\begin{aligned} \tilde{\theta}_{CW} &= \left(\frac{-5}{2 \cdot 1.9} \right) \{ -0.918(6) \cdot 6 + 1.000(8) \cdot 6 + 3.09(5) \cdot 6 \\ &\quad - 0.182(1) \cdot 12 + 0.258(1) \cdot 12 - 0.0504(4) \cdot 12 \} \\ &= -295(5) \text{ K}, \end{aligned} \quad (6)$$

a value very similar to the experimental value of $\theta_{CW} = -330 \text{ K}^{13}$ and in particular, $T_N = 291 \text{ K}^{12}$.

[†] Deceased 27 January 2015

¹ S. Sasaki, K. Fujino, and Y. TakÉchi, *Proc. Jpn. Acad. Ser. B Phys. Biol. Sci.* **55**, 43 (1979).

² M. Boiocchi, F. Caucia, M. Merli, D. Prella, and L. Ungaretti, *Eur. J. Minera.* **13**, 871 (2001).

³ L. Vegard, *Z. Phys.* **5**, 17 (1921).

⁴ W. J. L. Buyers, T. M. Holden, E. C. Svensson, R. A. Cowley, and M. T. Hutchings, *J. Phys. C Solid State Phys.* **4**, 2139 (1971).

⁵ D. I. Khomskii, *Transition Metal Compounds* (Cambridge University Press, 2014).

⁶ K. Lee, J. Lee, C. Lee, and M. Whangbo, *Bull. Korean Chem. Soc.* **35**, 1277 (2014).

⁷ J. Kanamori, *Progr. Theor. Phys.* **17**, 177 (1957).

⁸ R. A. Cowley, W. J. L. Buyers, C. Stock, Z. Yamani, C. Frost, J. W. Taylor, and D. Prabhakaran, *Phys. Rev. B* **88**, 205117 (2013).

⁹ J. Sakurai, W. J. L. Buyers, R. A. Cowley, and G. Dolling, *Phys. Rev.* **167**, 510 (1968).

¹⁰ F. Wallington, A. M. Arévalo-Lopez, J. W. Taylor, J. R. Stewart, V. García-Sakai, J. P. Attfield, and C. Stock, *Phys. Rev. B* **92**, 125116 (2015).

¹¹ H.-X. Deng, J. Li, S.-S. Li, J.-B. Xia, A. Walsh, and S.-H. Wei, *Appl. Phys. Lett.* **96**, 162508 (2010).

¹² W. Jauch, M. Reehuis, H. J. Bleif, F. Kubanek, and P. Pattison, *Phys. Rev. B* **64**, 052102 (2001).

¹³ T. Nagamiya, K. Yosida, and R. F. Kubo, *Adv. Phys.* **4**, 1 (1955).